Available online at www.sciencedirect.com

SciVerse ScienceDirect

Ceramics International 39 (2013) 791–800

CERAMICS INTERNATIONAL

www.elsevier.com/locate/ceramint

Laboratory scale study of the degradation of mullite/corundum refractories by reaction with alkali-doped deposit materials

J. Stjernberg[a,b,*], M.A. Olivas-Ogaz[a], M.-L. Antti[a], J.C. Ion[a], B. Lindblom[b]

[a]*Division of Materials Science, Luleå University of Technology, 971 87 Luleå, Sweden*
[b]*LKAB, 971 28 Luleå, Sweden*

Received 9 May 2012; received in revised form 29 June 2012; accepted 29 June 2012
Available online 13 July 2012

Abstract

Refractory bricks based on mullite and corundum, commonly used in rotary kilns for iron ore pellet production, and deposit material from an iron ore pellet production kiln, were used in laboratory scale tests to investigate refractory/deposit reactions and the infiltration of deposit components into the refractory bricks. The materials tested were in both monolithic form and in the form of powder. Alkali metal carbonates (containing sodium and potassium) were used as corrosive agents, to increase reaction kinetics. The morphological changes and active chemical reactions at the refractory/deposit interface in the samples were characterized by scanning electron microscopy. X-ray diffraction showed that alkali metals react with the mullite in the bricks, this being more pronounced in the case of sodium than potassium. Phases such as nepheline ($Na_2O \cdot Al_2O_3 \cdot 2SiO_2$), kalsilite and kaliophilite (both $K_2O \cdot Al_2O_3 \cdot 2SiO_2$), and leucite ($K_2O \cdot Al_2O_3 \cdot 4SiO_2$) were formed as a consequence of reactions between alkali metals and the refractory bricks. The formation of these phases causes volume expansions of between 20% and 25% in the brick materials, which accelerate degradation.

Keywords: Mullite; Refractories; Scanning electron microscopy; X-ray diffraction

1. Introduction

The hot manufacturing processes of making and shaping different metals would not be possible without refractories, which are used to protect furnaces and equipment against thermal, mechanical and chemical degradation mechanisms. In 2008, 42 Mt of refractories was produced globally [1]. Most of the refractories produced are based on alumina (Al_2O_3) and silica (SiO_2), as these are the most abundant oxides in the lithosphere [2]; they also possess good refractory properties, especially in mixtures.

Alumina and silica present in a ratio of 3:2 form the mineral mullite during heat treatment, which has favourable refractory properties, i.e. a high melting temperature, low thermal expansion coefficient and low thermal conductivity. Mullite was first described by Bowen and Grieg in 1924 [3], who also proposed the name according to its rare natural occurrence on the Scottish island of Mull. It is a solid solution with a wide variation of composition, however, it is commonly expressed stoichiometrically by the oxide formula $3Al_2O_3 \cdot 2SiO_2$ [4]. In refractories, mullite often appears as fine-grained needles in a glassy matrix, together with alumina and/or silica. However, even though mullite is considered to be an appropriate candidate material for refractory liners, there are more determinant parameters that are used to evaluate refractory properties: the amount of glassy phase determines e.g. creep behaviour [5]; the amount of porosity and purity of the grain boundary phase determine e.g. corrosion resistance [6], and the matching of the coefficient of thermal expansion (CTE) among different phases present in the refractory determines the ability to resist e.g. thermal shock [7].

The main consumer of refractories is the iron and steel industry. Iron ore is still one of our most important natural resources with ~1.600 Mt mined globally in 2010 [8]. Mined iron ore can be used directly as lump ore, or converted to e.g. pellets, to be reduced either by direct reduction or in a blast furnace. During pelletising of iron ore, the ore is first crushed

*Corresponding author LKAB, 971 28 Luleå, Sweden
Tel.: +46 70 9301 355.
E-mail addresses: jesper.stjernberg@ltu.se, jesper.stjernberg@lkab.com (J. Stjernberg).

0272-8842/$36.00
http://dx.doi.org/10.1016/j.ceramint.2012.06.094

into a powder, mixed with additives and a binder, and rolled into green balls (9–15 mm in diameter) that are sintered to pellets in a furnace [9]. The grate–kiln process can be used to achieve the required induration in the pellets, where the grate is a roaster furnace and the kiln is a rotating furnace. This system combines the advantages of the travelling grate and a rotary kiln. When the burden is in the form of magnetite, the rotary kiln achieves more uniform oxidation [10].

Rotary kilns were originally developed for the production of Portland cement. Besides cement production, rotary kilns are used for drying or sintering in many different applications, e.g. lime regeneration, heat treatment of hazardous waste, or refinement and processing of raw minerals, such as iron ore. Kiln design varies with application [11]. A typical rotary kiln, used in iron ore pellet production, can have a length of 40 m, a diameter of 7 m, and is fired by coal or natural gas. The refractory lining comprises bricks, most often based on Al_2O_3 and SiO_2. Such bricks deteriorate in use by a variety of mechanisms and must be replaced regularly. Alkali metal oxides and salts are known to act corrosively on the lining, even when present in small concentrations [12,13]. Thermal shock at starts and stops in operation together with mechanical strain may cause urgent stops in production, as bricks fall out [14]. Different Al_2O_3 concentrations in the refractories are used at different production sites and at different positions in the kilns. Sometimes concentrations as high as 90% are used, to increase the refractive properties of the bricks; then to avoid thermal spalling, the porosity is increased, which can lead to higher infiltration.

The Swedish mining company LKAB (Loussavaara Kiirunavaara Limited) uses the grate–kiln process in four of their six pellet plants. These kilns are lined with chamotte-based refractory bricks in the initial stage of their length, while a bauxite-based brick (with a higher alumina content) is used in the hotter remainder of the kiln. The two types of refractory brick studied are made from a basis of chamotte and bauxite. Mullite ($3Al_2O_3 \cdot 2SiO_2$) and corundum (Al_2O_3) are formed when the bricks are manufactured; they also contain traces of cristobalite, quartz (both SiO_2), and oxides of Ca, Fe, Ti and alkali metals. However, the chemical composition in the bricks varies slightly between production batches, as do the concentrations of phases present. However, by knowing the approximate chemical compositions of the bricks and the deposit material, the phases and minerals that originate from the original brick can be distinguished from those that evolve during the experiments carried out in this study.

Earlier laboratory scale based studies [15] found no pronounced reaction between the bauxite-based refractory material and the deposit material that accumulates in chunks on the refractory lining in the industrial kiln. However, the kinetics of degradation mechanisms in the refractories could be accelerated on the laboratory scale by adding Na_2CO_3. It was also observed that potassium is more reactive with the bricks than sodium [16], which justifies further studies with potassium additions. Azarenkova et al. [17] reported that Fe_2O_3 (hematite) enhances the reaction between mullite and alkali, which justifies the presence of Fe_2O_3 in the present study. The objective of this study was therefore to compare the infiltration depths of Na, K and hematite in the refractory bricks and their influence on the degradation process. Hematite in the form of deposit material was chosen to achieve similar conditions to those in an industrial kiln. In this paper, we report on studies of reactions occurring between refractory bricks and deposit material carried out on the laboratory scale.

2. Experimental procedure

2.1. Materials

The refractory materials used in the experiments were obtained from Höganäs Bjuf AB, (Bjuv, Sweden) in the form of bricks, which were machined to appropriate sizes for reaction tests in the laboratory scale furnace. For differential scanning calorimetry (DSC) and X-ray diffraction (XRD) analysis (see below), they were milled into a powder using a rod milling technique. Two different brick types were used; one was produced from a base of bauxite and the other from a base of chamotte. The chemical compositions of these bricks (according to data from the manufacturer) are shown in Table 1, represented as the most stable oxides.

The deposit material used in this study was collected from the outlet of a production kiln located in Kiruna, Sweden (labelled KK2), during a production stop (October 16, 2007). The compositions of the deposit material are shown below. The additives used were K_2CO_3 and Na_2CO_3 (both from Merck, 99.9 wt% purity).

2.2. Heat treatment

Three similar powder mixtures of equal amounts (by weight) of milled brick (bauxite-based) and deposit material, with an addition of 5 wt% K_2CO_3, were heat treated in air at 700, 1150 and 1350 °C (using a heating rate of 10 °C/min, and a cooling rate of 20 °C/min). These powders were subsequently analysed by XRD.

Refractory bricks (in as received condition) were machined to $125 \times 50 \times 20\ mm^3$ and heat treated in a laboratory furnace with 5 g of milled deposit material in two mounds on their surfaces (containing 10 wt% each of Na_2CO_3 and K_2CO_3). These samples were heat treated

Table 1
Nominal chemical compositions (wt%) of two commercial refractory bricks used in the experiments, based on manufacturer's data.

	Bauxite-based brick	Chamotte-based brick
Al_2O_3	~73	~58
SiO_2	~26	~36
CaO	0.2	0.3
TiO_2	2.7	2.1
Fe_2O_3	1.1	1.4
Alkalis	0.3	1.3

for 24 h at 1350 °C using a heating rate of 10 K/min. Subsequently the samples were sectioned to facilitate further investigation. Selected surfaces were polished prior to microscopical analysis.

2.3. Chemical analysis of deposit material

Chemical analysis of the deposit material was performed by X-ray fluorescence spectroscopy (XRF) in a PANalytical MagiX instrument using rhodium X-ray radiation, proportional flow counters for Na, Mg and Al, and a scintillation counter for all other elements. Prior to analysis, the sample was formed into a fused bead using a Herzog HAG 12 inductive fusion machine. The different valence states of iron (Fe^{2+} and Fe^{3+}) were differentiated using a titration method with potassium dichromate (ISO 9035). These analyses were performed at LKAB, Malmberget, Sweden.

2.4. Differential scanning calorimetry

Differential scanning calorimetry/thermal gravimetry (DSC/TG) experiments were carried out in an alumina-lined Pt–Rh furnace (Netzsch STA 449C Jupiter) equipped with a mass spectrometer (Netzsch Aeolos QMS 403C) through a heated (200 °C) glass capillary transfer line. The study was performed using powder mixtures in alumina crucibles between room temperature and 1350 °C (using a heating rate of 10 °C/min, and a cooling rate of 20 °C/min) in an air atmosphere (21% O_2 and 79% N_2). The sample contained a powder mixture of equal amounts of milled brick (bauxite-based) and deposit material (by weight), with an addition of 5 wt% K_2CO_3 (similar to the mixtures heat treated for XRD). The powder samples were compacted into a pellet by cold isostatic pressing (CIP) at 250 MPa prior to insertion into the instrument.

2.5. Microscopy

The microstructures of the heat treated brick–slag reaction zones were studied using a Moritex MS-500C optical microscope (OM), and a scanning electron microscope equipped with an X-ray energy dispersive detector (SEM/EDX: JEOL JSM-6460, Oxford Instruments, software INCA).

2.6. X-ray diffractometry

X-ray diffractometry (XRD) was carried out on powders of milled as-fabricated refractory bricks, and heat treated powder mixture samples. XRD was also carried out directly on the sample surfaces from the solid brick reaction tests, where samples were ground and analysed, layer by layer through the reaction zones, as shown in Fig. 1. The samples were ground 0.5 mm each time prior to the following XRD scan, except in the case of the chamotte-based brick with potassium addition, which was first ground 0.3 mm and thereafter in intervals of 0.5 mm. (Scans from intermediate layers in which no changes from previous layer were observed are not shown in the results.) All the X-ray diffraction experiments were conducted using a Philips X-ray diffractometer (MRD), and Cu Kα radiation (40 kV; 45 mA). The diffractograms were obtained over a 2θ interval between 10° and 90°.

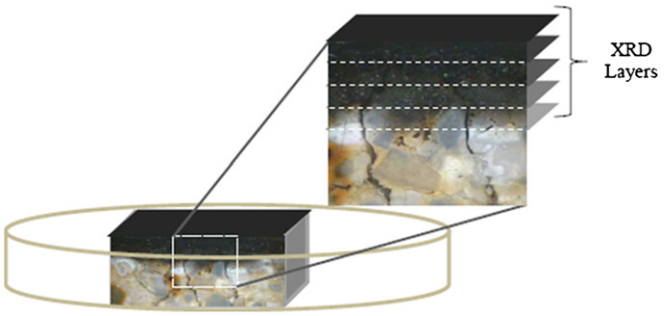

Fig. 1. Schematic of layer by layer scanning of solid brick samples by X-rays and recording of diffractograms.

3. Results

3.1. XRD of brick material

The X-ray diffractogram (not shown) from the as-fabricated brick material indicated that the bricks consisted predominantly of mullite and corundum, with traces of cristobalite and quartz. The other phases present were below the detection limit of the apparatus, or were amorphous.

3.2. Chemical analysis of deposit material

Chemical analysis of the deposit material collected in the industrial kiln, and used in the experiments, was carried out by XRF. Results are shown in Table 2.

As seen in Table 2, the deposit material is dominated by iron oxide, silicon oxide, and aluminium oxide, with traces of other oxides.

3.3. Reaction tests with powders

Fig. 2 shows the DSC and TG thermograms for a powder mixture of equal amounts (by weight) of milled brick and deposit material with the addition of 5 wt% K_2CO_3. The TG response (dashed line) shows a total mass loss of 1.8% between room temperature and 1350 °C. The sample first gains 0.3% in mass up to 80 °C as a result of the buoyancy effect. Subsequently, mass loss occurs continuously between 110 and 910 °C, being most pronounced between 110 and 170 °C, and between 650 and 910 °C. The DSC response (solid line) shows an endothermic peak at 910 °C. *In-situ* mass spectrometry shows emission of water and CO_2 at 115 °C, and emission of CO_2 between 500 and 800 °C both corresponding to mass losses.

Table 2
Composition of deposit material (wt%) collected from the outlet of a production kiln. (KK2), shown as the most stable oxides.

Fe_2O_3	Fe_3O_4	SiO_2	Al_2O_3	MgO	CaO	TiO_2	Na_2O	K_2O	V_2O_5	MnO	P_2O_5
89.2	0.91	5.41	2.43	0.60	0.58	0.23	< 0.05	0.16	0.17	0.06	0.12

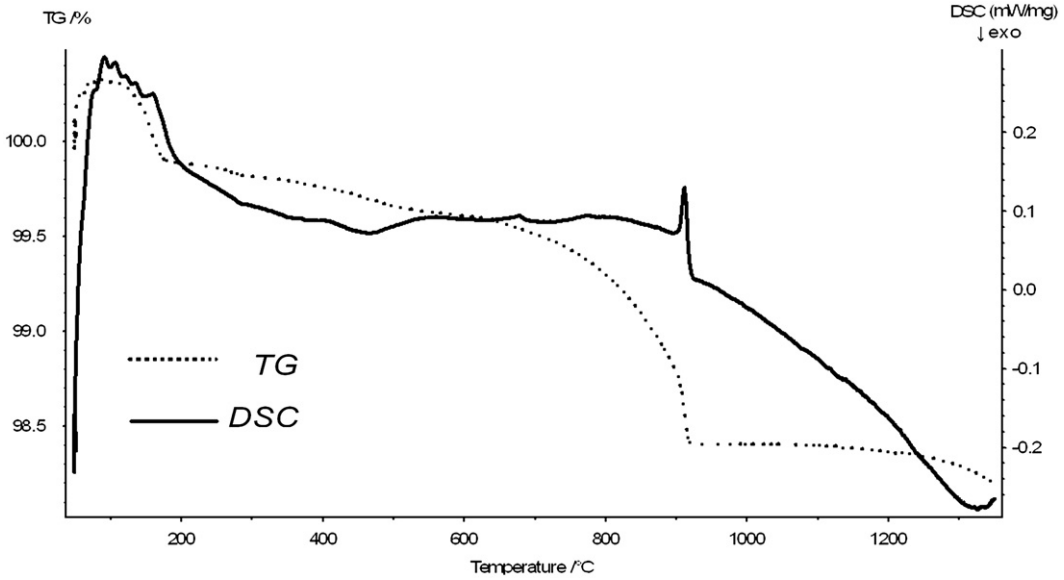

Fig. 2. DSC and TG thermograms of a heated powder mixture of equal amounts of brick and deposit material, with an addition of 5 wt% K_2CO_3 heated to 1350 °C.

Fig. 3 shows diffractograms from similar powder mixtures (equal amounts of brick and deposit material, with an addition of 5 wt% K_2CO_3), heat treated in an air atmosphere at 700, 1150 and 1350 °C, in order to clarify the reactions observed during thermal analysis.

The XRD results showed that kalsilite ($K_2O \cdot Al_2O_3 \cdot 2SiO_2$) forms between 700 and 1150 °C. The experiment performed with a sample heated to 1350 °C showed that the amount of kalsilite decreased; instead leucite ($K_2O \cdot Al_2O_3 \cdot 4SiO_2$) is formed. All other peaks correspond to phases present in the deposit material (hematite), and brick material (corundum, quartz and mullite), except the unmarked peak at 44.5°, which corresponds to the aluminium sample holder.

3.4. Reaction tests with solid brick material

Fig. 4 shows an image from the reaction test using the solid brick (chamotte-based) with milled deposit material placed in mounds on it. It can be seen that a more pronounced reaction took part in the mound containing the sodium addition, than that containing the addition of potassium. A higher concentration of liquid phase had been present in the mound containing sodium, while the mound with potassium remained mainly in the solid form. With the sodium addition, the reaction zone migrated into the brick, whereas only a minor amount of material from the mound with potassium penetrated the brick (the sintered mound could easily be removed from the brick). This was the case for both brick types.

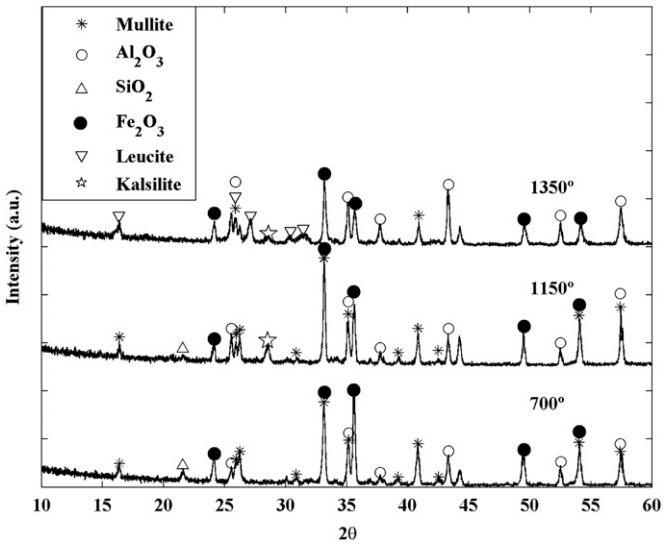

Fig. 3. Diffractograms of heated powder mixtures of equal amounts of brick and deposit material with an addition of 5 wt% of K_2CO_3, heated in air to 700, 1150 and 1350 °C.

3.4.1. Bauxite-based brick: reaction with sodium-doped deposit material

The deposit material containing sodium was more reactive than that containing potassium: the visual corroded layer was 3.5 mm, as seen in Fig. 5. XRD scans carried out at depths of 0, 1.5, 2.5, and 3.5 mm in the brick are shown in Fig. 6. A summary of the phases present at different depths from the different tests is given in Table 3.

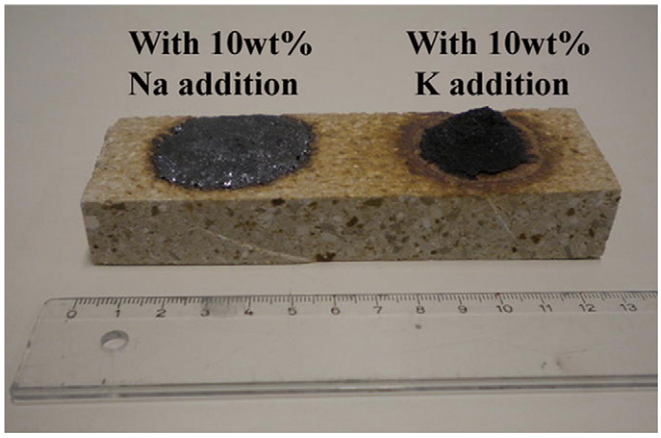

Fig. 4. Chamotte-based brick after the solid brick reaction test.

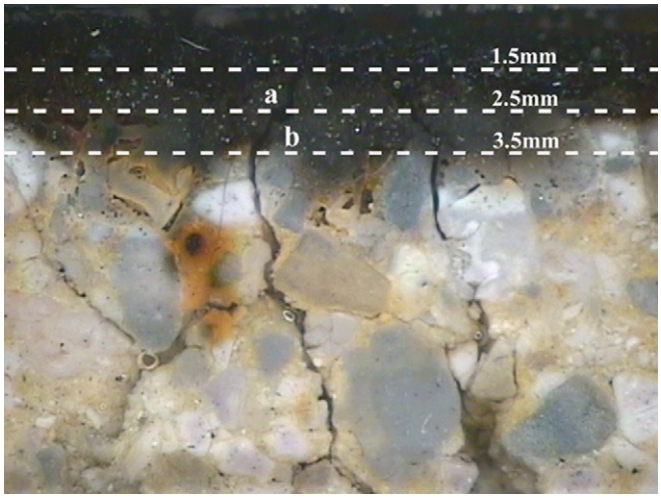

Fig. 5. Optical micrograph showing the reaction zone from the solid brick reaction test with the bauxite-based brick and sodium-doped deposit material.

Fig. 7(a), which corresponds to the area marked "a" in Fig. 5, shows hematite grains (marked H) with sizes from ~10 μm to above 100 μm, which remained on the newly formed deposit/refractory interface in a distinct front. Grains of corundum (marked C), with dimensions that decreased towards the interaction zone, were depleted in titanium. Instead titanium, together with iron oxide, forms shells on these grains, marked with small white arrows. Some hematite (marked H) grains have varying concentrations of aluminium and titanium, and therefore a variation in brightness resulting from the composition contrast of the backscattered signal. The black arrow shows such a grain. Fig. 7(b), which corresponds to the area marked "b" in Fig. 5, shows grains of mullite (marked M) and corundum (marked C) deeper in the brick. All phases were detected by EDS.

3.4.2. Bauxite-based brick: reaction with potassium-doped deposit material

Little reaction between the deposit material containing potassium and the brick material was observed, in comparison with the test comprising sodium; the visual

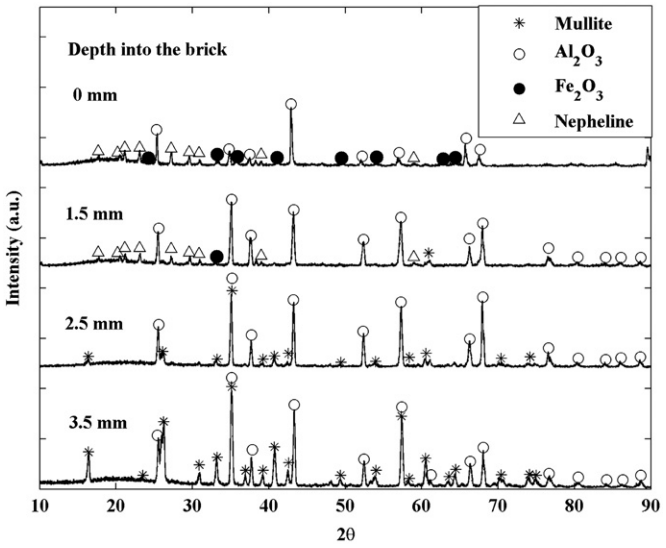

Fig. 6. Diffractograms obtained from surfaces ground and polished to various depths in the bauxite-based refractory brick.

corroded layer was only ~0.2 mm in thickness, as seen in Fig. 8. XRD scans carried out at depths of 0, 0.5 and 1 mm in the refractory brick are shown in Fig. 9.

Fig. 10(a) shows how voids are filled with a silica–potassium glass (marked with arrows), which at some locations penetrated the brick to a depth of ~0.5 mm. These glassy fill-ups of voids were observed as protrusions of the corroded layer (close to "a" in Fig. 8), and has an average chemical composition of (in wt%, detected by EDS): 38% O, 30% Si, 15% K, 10% Fe, 5% Al, and 1% each of Na and Ti. The surrounding bulk material (within 0.3 mm from the surface) however, has an average composition of 33% O, 25% K, 17% Fe, 12% Al, 10% Si, and 3% Ti. Moreover, the penetration front of potassium causes the formation of secondary mullite from primary mullite, marked with a rectangle in Fig. 10(a), and shown with a higher magnification in Fig. 10(b) (secondary mullite marked S, primary mullite marked P).

3.4.3. Chamotte-based brick: reaction with sodium-doped deposit material

The deposit material containing sodium was more reactive than that doped with potassium, and the visual corroded layer was 2.5 mm, shown in Fig. 11. XRD scans carried out at depths 0, 0.3, 1.3 and 2.3 mm in the refractory brick are shown in Fig. 12.

Fig. 13(a) shows hematite grains (marked H) with sizes ~50 μm that remain on the newly formed deposit/refractory interface in a distinct front. Fig. 13(b) shows how fine grained hematite (~2 μm, marked with small arrows) has migrated into the bulk of the refractory brick, and is found together with mullite rods (marked M).

3.4.4. Chamotte-based brick: reaction with potassium-doped deposit material

The deposit material containing potassium reacted little with the brick material, compared with the test using

Table 3
Phases determined by XRD at different depths in both brick types. Abbreviations are used as follows: C (corundum); M (mullite); H (hematite); N (nepheline); K (kaliophilite); L (leucite) and A (amorphous).

Depth [mm]	Bauxite with Na	Bauxite with K	Chamotte with Na[a*]	Chamotte with K
0	C, H, N	C, H, K, A	C, H, N, A	C, H, K, L, A
0.5	–	C, M, K, A	C, H, N, A	C, M, K, L
1	–	C, M, K, A	–	C, M, A
1.5	C, H, N	–	C, M, H, N, A	–
2	–	–	–	–
2.5	C, M	–	C, M, A	–
3	–	–	–	–
3.5	C, M	–	–	–

[a*]All observations at a depth 0.2 mm less than that indicated in Table 3, see text.

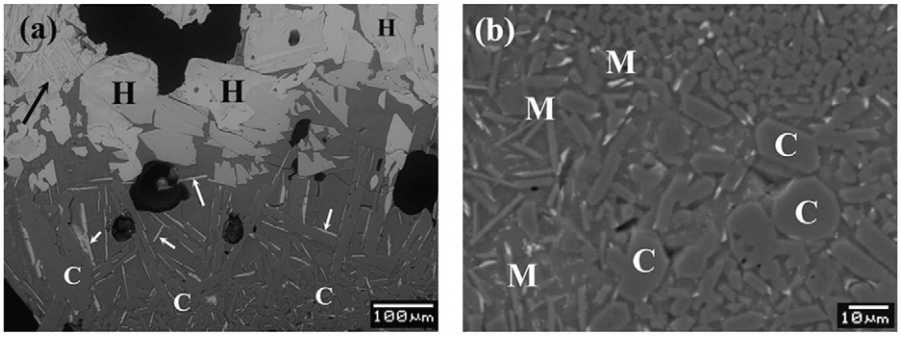

Fig. 7. SEM micrographs, showing (a) the interaction zone between refractory and deposit, and (b) mullite and corundum grains deeper in the refractory brick. H = hematite, C = corundum, M = mullite.

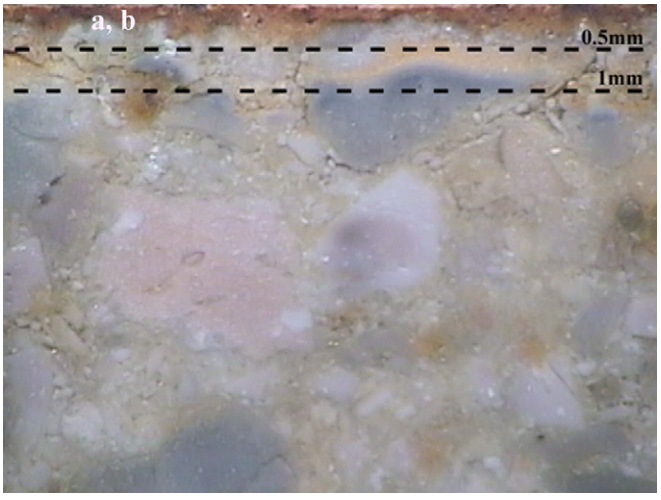

Fig. 8. Optical micrograph showing the reaction zone from the solid brick reaction test with the bauxite-based brick and potassium-doped deposit material.

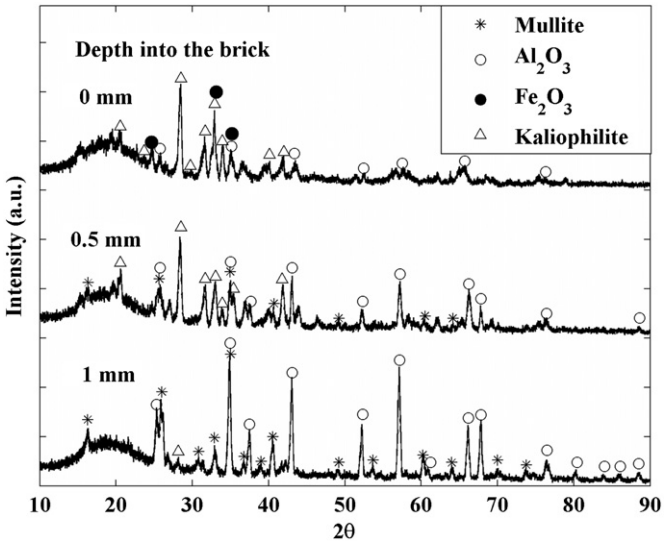

Fig. 9. Diffractograms obtained from surfaces ground and polished to various depths in the bauxite-based refractory brick.

sodium; the visual corroded layer was just ~0.2 mm in thickness, as seen in Fig. 14. XRD scans carried out at depths of 0, 0.5 and 1 mm in the refractory brick are shown in Fig. 15.

The SEM micrograph in Fig. 16(a) was taken just beneath the deposit/refractory brick interface. In this brick, the migration front of potassium was evenly distributed: voids filled with liquid were not observed (possibly because of the lower porosity of this brick). Potassium migrates by solid state diffusion along grain boundaries and through the glassy phase, and its presence transforms the primary mullite to secondary mullite. Behind this front, kaliophilite and leucite are formed; however, most of the potassium is found in the glassy phase. The grains are marked: P (primary mullite);

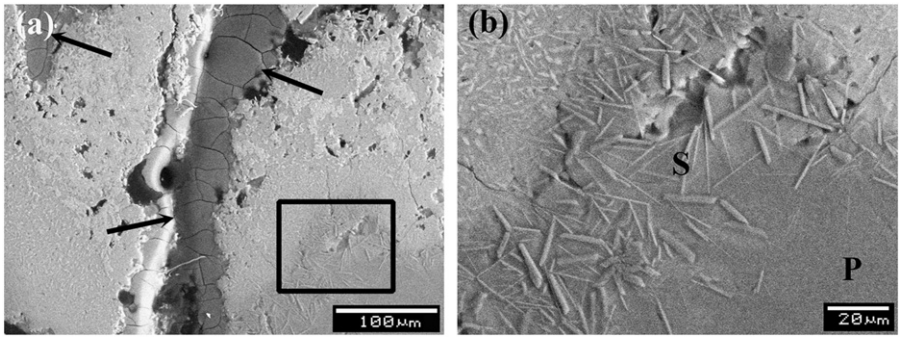

Fig. 10. SEM micrographs, showing (a) how voids in the refractory brick are filled with a silica–potassium glass (marked with arrows), and (b) how secondary mullite is formed. P=primary mullite, S=secondary mullite.

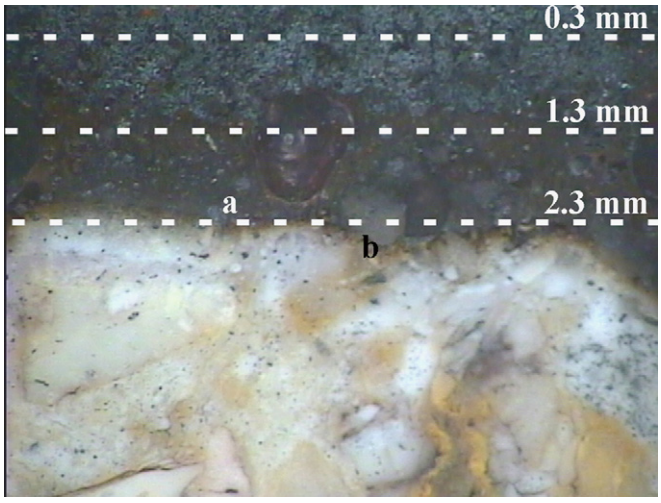

Fig. 11. Optical micrograph showing the reaction zone from the solid brick reaction test with the chamotte-based brick and sodium-doped deposit material.

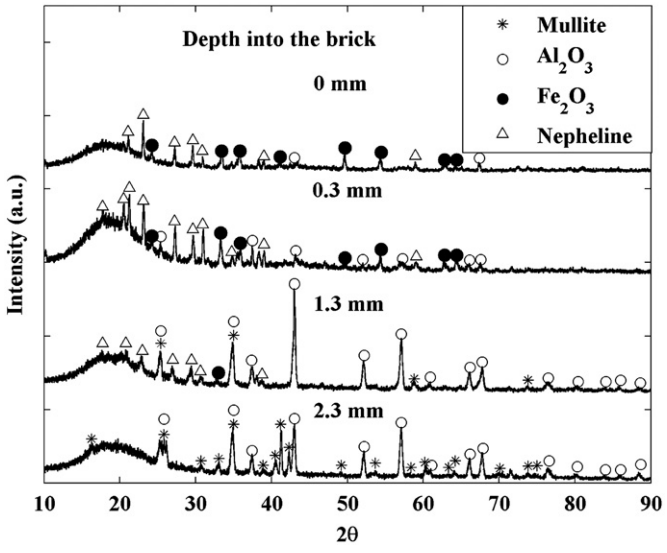

Fig. 12. Diffractograms obtained from surfaces ground and polished to various depths in the chamotte-based refractory brick.

S (secondary mullite); C (corundum) and K (kaliophilite); all detected by EDS. Arrows close to the surface mark precipitation of hematite in the refractory brick. The SEM micrograph in Fig. 16(b) shows the formation of secondary mullite in the brick.

3.4.5. *Summary of XRD analysis*

Table 3 summarises the phases present at different depths in both brick types, in the presence of sodium and potassium. Abbreviations are used as follows: C (corundum); M (mullite); H (hematite); N (nepheline); K (kaliophilite); L (leucite) and A (amorphous). Results from intermediate layers where no changes from previous layer were detected are not shown.

4. Discussion

This paper deals with high temperature reactions and infiltration mechanisms of components from deposit materials into mullite-corundum bricks based upon a laboratory-scale study. The effects of potassium and sodium are observed to be distinctly different, even if they both are often generalised as *alkalis*.

The presence of Na_2CO_3 in the deposit material leads to the formation of a smelted phase. The effect of the presence of K_2CO_3 in the deposit material is that the deposit material maintains a solid form. Further, in the presence of sodium, hematite from the deposit material migrates into the partially dissolved brick material to a depth of several millimeters. In the presence of potassium, little of the hematite in the deposit material penetrates the brick surface, while potassium penetrates the brick to a depth of approximately 1 mm. However, sodium-feldspathoid (nepheline) is found only in the corroded layer accompanied with hematite, while potassium-feldspathoids (kaliophilite and leucite) are found beneath the corroded layer in the refractory brick. This is in agreement with Narita et al. [18] who observed that potassium was found in concentrations five times as high in the fireclay based refractory lining of a blast furnace (which is comparable in composition with the chamotte-based refractory brick used in this study). It appears that while potassium penetrates

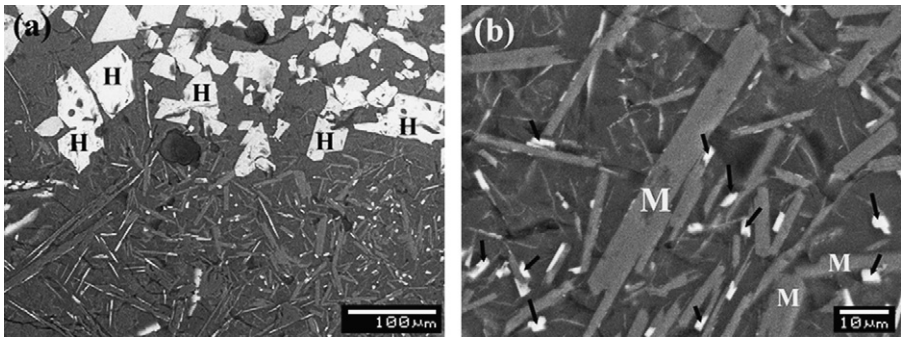

Fig. 13. SEM micrographs, showing (a) hematite grains with sizes ~50 μm that remain on the refractory surface in a distinct front, while (b) shows how fine grained hematite (~2 μm) has migrated into the bulk of the refractory brick. H = hematite, M = mullite.

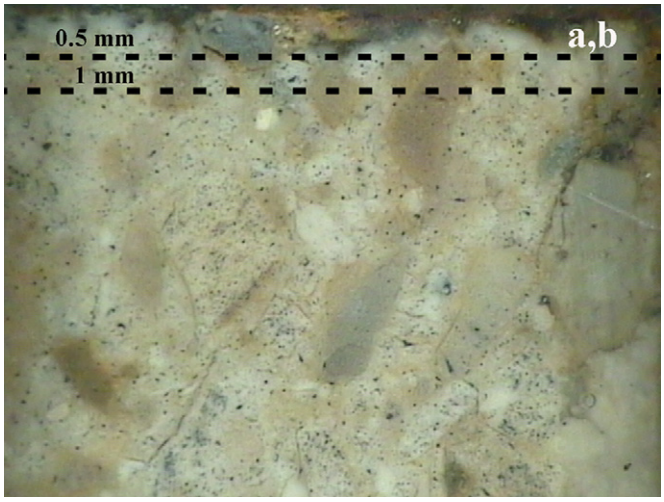

Fig. 14. Optical micrograph showing the reaction zone from the solid brick reaction test with the chamotte-based brick and potassium-doped deposit material.

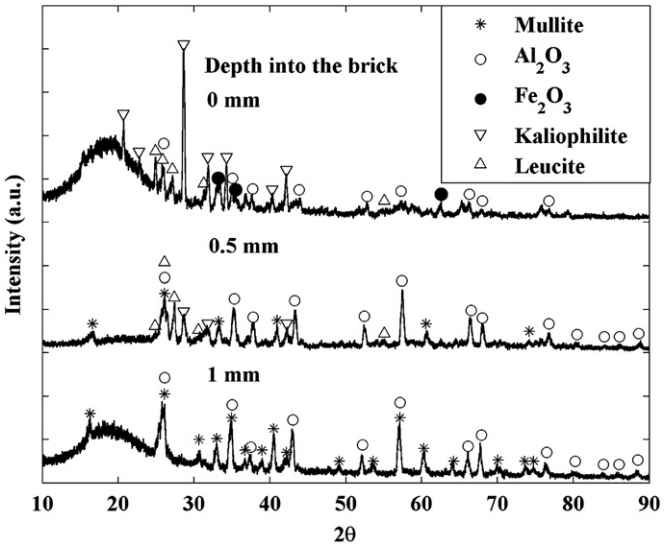

Fig. 15. Diffractograms obtained from surfaces ground and polished to various depths in the chamotte-based refractory brick.

deeply into the uncorroded refractory bricks (mainly by capillary infiltration and solid state diffusion along grain boundaries and through a glassy phase) and reacts with mullite and corundum, sodium reacts only with the refractory brick (mainly in its liquid state), in a more aggravating manner at the refractory surface.

In the reaction tests with powders, kalsilite forms between 700 and 1150 °C. Kalsilite is partially depleted at 1350 °C, to the benefit of leucite ($K_2O \cdot Al_2O_3 \cdot 4SiO_2$) which forms in larger concentrations than kalsilite. Scudeller et al. [19] suggested that K_2O starts to react with SiO_2, forming a glassy matrix. With time, kaliophilite ($K_2O \cdot Al_2O_3 \cdot 2SiO_2$), a cubic form of kalsilite, is formed; at longer times and depending on the SiO_2 available, leucite ($K_2O \cdot Al_2O_3 \cdot 4SiO_2$) is formed. Moreover, Zhang et al. [20] observed the activation energy for kalsilite crystallisation to be 103 kJ/mol, while 125 kJ/mol was observed for leucite, which further explains why kalsilite forms first.

Secondary mullite in a glassy phase is formed from primary mullite at a depth of ~300 μm in both the bauxite-based- and the chamotte-based brick, in contact with potassium. At a depth of 500 μm, kaliophilite co-exists with the mullite in both brick types. The observation of secondary mullite in needle-like formations in an alkali rich glass is in agreement with earlier observations. Lundin [21] and Schüller [22] first described two different types of mullite of different morphologies from studies of porcelain. On the laboratory scale it was observed by Iqbal and Lee [23,24] and Lee and Iqbal [25] that primary mullite was first formed in an amorphous silica glass from heated mixtures of clays, silica sand and potash feldspar, while the alumina richer secondary mullite started to grow from primary mullite in needle shaped formations, in the presence of an amorphous alkali-aluminosilicate. The formation of secondary mullite from primary mullite has also been observed in studies of refractory bricks used in an industrial scale rotary kiln [13]. Moreover, Schüller [22] observed that formation of secondary mullite was affected by the presence of potash feldspar and silica, and in contrast to this, soda feldspar caused the same action at higher temperatures.

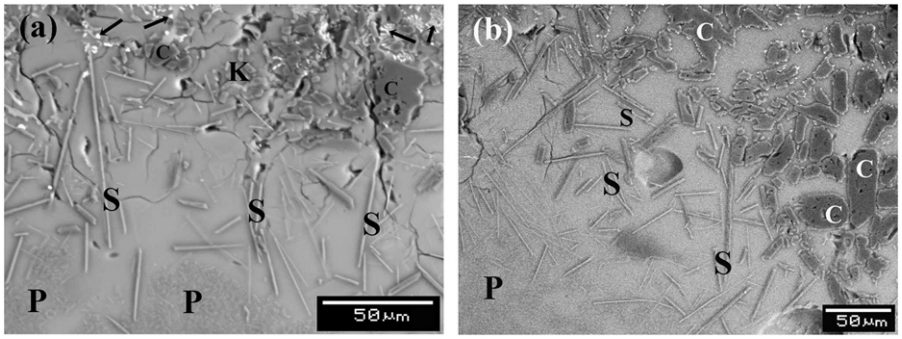

Fig. 16. SEM micrographs showing (a) formation of secondary mullite and kaliophilite in the refractory brick, and (b) formation of secondary mullite in the refractory brick. Arrows mark precipitated hematite. K = kaliophilite, C = corundum, P = primary mullite, S = secondary mullite.

It can be assumed that the transformation of primary mullite to secondary mullite precedes the transformation to kaliophilite, which is likely to be the phase seen as small needles above the secondary mullite in the SEM micrograph in Fig. 16(a). The disintegration of mullite that results in the formation of feldspathoid minerals is associated with a volume expansion, observed previously by dilatometry [15], which can cause spallation by alkali bursting of the refractory lining. The formation of alkali metal containing phases causes volume expansions of between 20% and 25% in the brick materials, which accelerate degradation. Therefore, the formation of secondary mullite, caused by the presence of potassium around the aggregates of primary mullite in the refractories studied, is a degrading mechanism that finally promotes corrosion of the refractories. However, minor formations of feldspathoid minerals may create a dense layer that prevents degradation under certain conditions [16].

Kalsilite formed only in the reaction test with powders—kaliophilite (the cubic form of kalsilite) was instead formed in the solid brick reaction tests when potassium was involved. Also notable is an increased amount of leucite compared with kalsilite/kaliophilite, which is formed in the experiments using powders, compared with solid brick reaction tests. One explanation could be that as the powders are milled, the reaction paths are minimised compared with reactions with solid bricks. Moreover, leucite and kaliophilite are formed in the chamotte-based brick (in reaction tests with solid bricks), whilst only kaliophilite is formed in the bauxite-based brick. The higher amount of Si in the chamotte-based brick enables this leucite formation. The amorphous signal in diffractograms recorded from several samples, corresponds to a glassy phase and/or the epoxy resin in which the sample is mounted.

Grains of hematite with dimensions between 10 and 100 μm remain on the original interface between the brick and deposit material in the presence of potassium. Sodium dissolves the surface of the brick, causing the reaction zone to migrate to a depth of ~3 mm in both types of brick, and consequently grains of hematite migrate to that depth. However, micrometre sized hematite is to some extent found deeper in the refractory brick material, beneath the newly created reaction zone. It is not clear if this fine grained hematite has migrated into the brick material in its form as these grains, or if, which is more likely, it has diffused in the glassy phase as iron ions/atoms, and precipitated deeper in the brick as these grains. With similar materials it has also been observed previously, both in an industrial rotary kiln [13] and on the laboratory scale [15,16] that most of the hematite remains at the interface between the refractory brick and the deposit. However, it was also observed that hematite may migrate into the refractory brick, especially by capillary flow through voids, cracks, and brick joints, supported by the presence of alkali metals.

TiO_2 is present in both types of brick in concentrations around 2 wt%, mainly found together with corundum grains in as-fabricated bricks. It is shown in Fig. 7(a) how the titanium segregates from alumina, and instead forms a solid solution with iron oxide. This phenomenon has been observed previously [13,16], and may be explained by the fact that just a few percent aluminium ions can enter the TiO_2 lattice (at temperatures between ~1000 °C and ~1800 °C), while Al_2O_3 does not dissolve titanium ions at all [26].

Migration of alkali metals primarily occurs through pores, a glassy phase, and grain boundaries, and is observed to act corrosively on the refractory bricks. Addition of zircon ($ZrSiO_4$) to the binder phase appears to be a promising way to prevent corrosive mechanisms, both with mullite-based refractories exposed to alkali vapours [6] and with MgO–spinel refractories exposed to cement clinker [27]. It has also been used in zircon–zirconia composites, to make the ceramic composite denser [28]. A suggestion for further work is to evaluate the effect of zirconia addition to the refractories in this application.

5. Conclusions and future work

The results of the reaction tests using powders allow the following conclusions to be drawn:

- kalsilite forms from mullite between 700 and 1150 °C.
- between 1150 and 1350 °C the amount of kalsilite decreases, and instead leucite is formed.

The results of reaction tests with solid bricks and powders allow the following conclusions to be drawn:

- nepheline is formed in the corroded layer of the refractory brick, while potassium feldspathoids are found deeper in the solid brick;
- deposit material melts in the presence of sodium, but sinters in the presence of potassium;
- sodium acts in a more aggressive manner than potassium at the surface of the refractory bricks, while potassium penetrates deeper into the uncorroded refractory bricks, and in much higher concentrations than sodium;
- kaliophilite, the cubic form of kalsilite, is formed only in the solid brick reaction tests;
- secondary mullite and an increased amount of glassy phase are formed as a transition phase, prior to the formation of feldspathoid minerals;
- the formation of alkali metal containing phases causes volume expansions of between 20% and 25% in the brick materials, which accelerate degradation.

Future work could include dilatometric studies of volume expansion after corrosion tests.

Acknowledgements

The authors are grateful to Hjalmar Lundbohm Research Centre (HLRC) for financial support, to Xiaoyan Ji (Division of Energy Science, LTU) for translation of a paper written in Chinese, and to LKAB (Malmberget) for help with chemical analysis.

References

[1] I. Watanabe, Overview of refractory resources worldwide, Taikabutsu Overseas 30 (4) (2010) 227–233.
[2] A. Ronov, A. Yaroshevsky, Chemical composition of the earth's crust, American Geophysical Union Monograph 13 (1969) 37–57.
[3] N.L. Bowen, J.W. Grieg, The system $Al_2O_3 \cdot SiO_2$, Journal of the American Ceramic Society 7 (4) (1924) 238–254.
[4] H. Schneider, Structure and properties of mullite—a review, Journal of the European Ceramic Society 28 (2) (2008) 329–344.
[5] H. Ohira, M. Ismail, Y. Yamamoto, T. Akiba, Shigeyuki Somiya, Mechanical properties of high purity mullite at elevated temperatures, Journal of the European Ceramic Society 16 (2) (1996) 225–229.
[6] M. Baspinar, F. Kara, Optimization of the corrosion behaviour of mullite refractories against alkali vapour via $ZrSiO_4$ addition to the binder phase, Ceramics—Silikáty 53 (4) (2009) 242–249.
[7] C. Aksel, Mechanical properties and thermal shock behaviour of alumina–mullite–zirconia and alumina–mullite refractory materials by slip casting, Ceramics International 29 (3) (2003) 311–316.
[8] United Nations Conference on Trade and Development (UNCTAD), 2010, The Iron Ore Market 2009–2011.
[9] S.P.E. Forsmo, S.-E. Forsmo, P.-O. Samskog, B.M.T. Björkman, Mechanisms in oxidation and sintering of magnetite iron ore pellets, Powder Technology 183 (2) (2008) 247–259.
[10] Y. Zhang, J. Feng, J. Xu, Y. Zhang, J. Yang, Energy and exergy analyses of a mixed fuel-fired grate–kiln for iron ore pellet induration, Energy and Conversion Management 52 (5) (2011) 2064–2071.
[11] A. Boateng, Rotary Kilns—Transport phenomena and transport processes, Elsevier Inc., Burlington, ISBN 978-0-7506-7877-3, 2008.
[12] N. Dahotre, P. Kadolkar, S. Shah, Refractory ceramic coating: processes, systems and wettability/adhesion, Surface and Interface Analysis 31 (7) (2001) 659–672.
[13] J. Stjernberg, J.C. Ion, M.-L. Antti, L.-O. Nordin, B. Lindblom, M. Odén, Extended studies of degradation mechanisms in the refractory lining of a rotary kiln for iron ore pellet production, Journal of the European Ceramic Society 32 (8) (2012) 1519–1528.
[14] K. Zhu., C. Zhao, On increasing the lining lifetime of rotary kiln, Sintering and Pelletizing 28 (1) (2003) 24–25 in Chinese.
[15] J. Stjernberg, L.-O. Nordin, M.-L. Antti, M. Odén, Degradation of refractory bricks used as thermal insulation in rotary kilns for iron ore pellet production, International Journal of Applied Ceramic Technology 6 (6) (2009) 717–726.
[16] J. Stjernberg, B. Lindblom, J. Wikström, M.-L. Antti, M. Odén, Ceramics International 36 (2) (2010) 733–740.
[17] L.E. Azarenkova, B.N. Starshinov, N.V. Pitak, R.M. Fedoruk, M.V. Konoplya, Refractories and Industrial Ceramics 21 (5) (1980) 255–260.
[18] K. Narita, T. Onoye, Y. Satoh, M. Miyamoto, K. Taniguchi, S. Kamatani, T. Sato, S. Fukihara, Effects of alkalis and zinc on the wear of blast furnace refractories, ISIJ International 21 (12) (1981) 839–845.
[19] L. Scudeller, E. Longo, J. Varela, Potassium vapor attack in refractories of the alumina–silica system, Journal of the American Ceramic Society 73 (5) (1990) 1413–1416.
[20] Y. Zhang, M. Lv, D. Chen, J. Wu, Leucite crystallization kinetics with kalsilite as a transition phase, Materials Letters 61 (14–15) (2007) 2978–2981.
[21] S. Lundin, Electron microscopy of whiteware bodies, Transactions of the International Ceramic Congress 4 (1954) 383–390.
[22] K. Schüller, Reactions between mullite and glassy phase in porcelains, Transactions of the British Ceramic Society 64 (2) (1964) 103–117.
[23] Y. Iqbal, W. Lee, Fired porcelain microstructures revisited, Journal of the American Ceramic Society 82 (12) (1999) 3584–3590.
[24] Y. Iqbal, W. Lee, Microstructural evolution in triaxial porcelain, Journal of the American Ceramic Society 83 (12) (2000) 3121–3127.
[25] W. Lee, Y. Iqbal, Influence of mixing on mullite formation in porcelain, Journal of the European Ceramic Society 21 (14) (2001) 2583–2586.
[26] K. Das, P. Choudhury, S. Das, The Al–O–Ti (aluminum–oxygen–titanium) system, Journal of Phase Equilibria 23 (5) (2002) 525–535.
[27] R. Ceylantekin, C. Aksel, Improvements on corrosion behaviours of MgO–spinel composite refractories by addition of $ZrSiO_4$, Journal of the European Ceramic Society 32 (4) (2012) 727–736.
[28] N. Rendtorff, S. Grasso, C. Hu, G. Suarez, E. Aglietti, Y. Sakka, Zircon–zirconia ($ZrSiO_4$–ZrO_2) dense ceramic composites by spark plasma sintering, Journal of the European Ceramic Society 32 (4) (2012) 787–793.